



A Schiff base of 2-((E)-(2-amino-5-methylphenylimino)methyl)-5-(difluoromethoxy)phenol and its applications on fluorescent chemosensor for selection of Mg²⁺ ion, molecular docking, and anticancer activity

Iyappan Mathivanan, Dhineshkumar Ezhumalai, Anbuselvan Chinnadurai*

Department of Chemistry, Annamalai University, Annamalaiagar, India

ARTICLE INFO

Received on: 08/04/2020
Accepted on: 03/07/2020
Available online: 05/08/2020

Key words:

Schiff base, Mg²⁺ ion, colorimetric, Fluorometric, cytotoxicity, DFT.

ABSTRACT

A novel Schiff base of 2-((E)-(2-amino-5-methylphenylimino)methyl)-5-(difluoromethoxy)phenol (**R**) was synthesized and characterized by FTIR, ¹H&¹³C-NMR, and mass spectrometry. The receptor turned yellow and then green in the presence of Mg²⁺ molecules, with the intervention of different metal ions. The selectivity and sensitivity of Mg²⁺ ion caused the maximum fluorescence emission intensity at 524 nm, with an excitation wavelength at 378 nm. Further experiments confirmed that receptor **R** binds with Mg²⁺. Job's plot conforms to a 1:1 stoichiometry complex formation. The strong fluorescence is owing to the photoinduced electron/energy transfer effect. The receptor was recovered by an ethylenediaminetetraacetic acid titration and the emission intensity also returned to a value equivalent to the unbound ligand. protein data bank: 4J96 was used for the molecular docking of receptor **R**. The cytotoxicity effect treatment was carried out by increasing the concentration of HeLa cells to predict IC₅₀ value. The highest occupied molecular orbital/lowest unoccupied molecular orbital energy gap calculated and compared between **R** results as 3.48 eV and **R**-Mg²⁺ alpha and the beta value calculated a low energy value at 2.27 eV.

INTRODUCTION

The most important magnesium (Mg²⁺) ion, which is extremely abundant, is essential for a number of cellular processes, such as cell death, cell proliferation, biochemical reactions, enzyme-driven reactions, stabilization of DNA conformation channel regulation, and signal transduction (Liu *et al.*, 2018). A human body absorbing excess magnesium ions has side effects like nausea and diarrhea. The excess Mg²⁺ ions also results in age-related diseases and nervous disorders. It is with great interest that fluorescent chemical sensors are designed to detect Mg²⁺ ions (Tamil Selvan *et al.*, 2018). For instance, certain low levels of Mg²⁺ ions are related to the improvement of Parkinson's disease. As a consequence, the significance of Mg²⁺ in many physiological conditions necessitates

a new chemical apparatus to investigate Mg²⁺ ion in both health and disease (Treadwell *et al.*, 2018). Recently, numerous families of Mg²⁺ response with fluorescent chemosensors containing moiety-based ligand groups, including diketone, calyx, arene, crown ether, porphyrin, and (C = N) imine-like aromatic, have been formed in the region (Zhao *et al.*, 2014). The presence of magnesium ions in mineral water supply is relatively quantitative. This is usually carried out by the ethylenediaminetetraacetic acid (EDTA) complexometric titration due to the presence of Mg²⁺ in drinking water. On the contrary, this process is laborious, sensitive, and time-consuming, as well as it contains errors due to interference from numerous metal ions. However, the needed improvement and sensitivity of analytical types for Mg²⁺ ion is not so effective in this regard (Men *et al.*, 2015). Notably, fluorescence-based chemosensors provide real-time answers to a variety of lists that allow for complex measurements and easy handling. Significant efforts have, in recent times, been made to find new suitable fluorescent samples with all the desired properties, such as high sensitivity, selectivity, low-cost synthesis, aqueous solubility, and simple preparation (Orrego-Hernández *et al.*, 2016). The key

*Corresponding Author
Anbuselvan Chinnadurai, Department of Chemistry, Annamalai University, Annamalaiagar, India. E-mail: cas_amu@yahoo.co.in

advantage of fluorescent chemosensors, “turn-on” sensors compared to “turn-off” sensors, is that it clearly detects a low concentration than a “black” setting, which decreases the probability of false-positive signals and improves sensitivity, depending on the number of studies carried out. Moreover, colorimetric chemosensors have attracted much attention because it allows “naked-eye” detection, which is not complicated and expensive. These behaviors contribute to quantitative and qualitative information (Li *et al.*, 2014). A variety of signaling mechanisms targeting the optical detection of different organisms were developed and implemented. The photoinduced electron/energy transfer (PET) signaling pathways consist of excimers and exciplex formations (Kim *et al.*, 2002), the excited state of intramolecular and intermolecular proton transfers (Beer *et al.*, 1998), metal–ligand charge transfer (MLCT) Kim and Yoon, 2002), intramolecular charge transfer (Xu *et al.*, 2005), and closed-queuing network isomerization (Wu *et al.*, 2007). The fluorescence sensors designed for metal ions have a huge significance these days. PET has been broadly used as a tool in such aspects. Many compounds contain amine and amide moiety or result in fluorescence quenching via PET by electron donating and accepting sites within the molecule. These group categories are called PET process chemosensors for “on–off” signals. Fluorescence quenching via PET due to structural flexibility (there is an unregulated torsional rotation between carbon–carbon bond which is covalently linked to two units) in these sensors is responsible for intramolecular rotation wherein a charge transfer to an excited single state is swiftly disabled (Gupta *et al.*, 2018). Schiff base ligands, also called as “privileged ligands”, are obtained by the condensation of aldehydes and amines prepared by a well-known procedure that is effective for various metal ions in different oxidation states. The efficiency of the Schiff base–metal complex is realized by their use and application across a range of fields, from catalysis to medicine and fluorescent chemosensors (Gao *et al.*, 2018). Schiff base methods of binding metal complexes are briefly studied in the literature (Abu-Dief and Mohamed, 2015) due to their antioxidant activities (Li and Yang, 2009; Liu and Yang, 2009; Tarafder *et al.*, 2001), antitumoral properties (Adsule *et al.*, 2006; Jana *et al.*, 2016), antimicrobial activity (Parashar *et al.*, 1988; Raman *et al.*, 2001), catalytic activities (Jia and Li, 2015; Mouri *et al.*, 2010), and photophysical properties (Cozzi *et al.*, 2003; Ziółek *et al.*, 2008).

In this article, Scheme 1 shows the synthesis of compound **R** of 2-((E)-(2-amino-5-methylphenylimino)methyl)-5-(difluoromethoxy)phenol and mentions its use as a chemosensor

for high sensitivity and selectivity toward Mg^{2+} ions in different metals envisaged in this experiment. Magnesium was proposed by titration with additional metal ions and theoretical calculations. Moreover, the ligand **R** complexation with Mg^{2+} ion was confirmed by EDTA titration and the cytotoxicity activity is related to molecular docking studies.

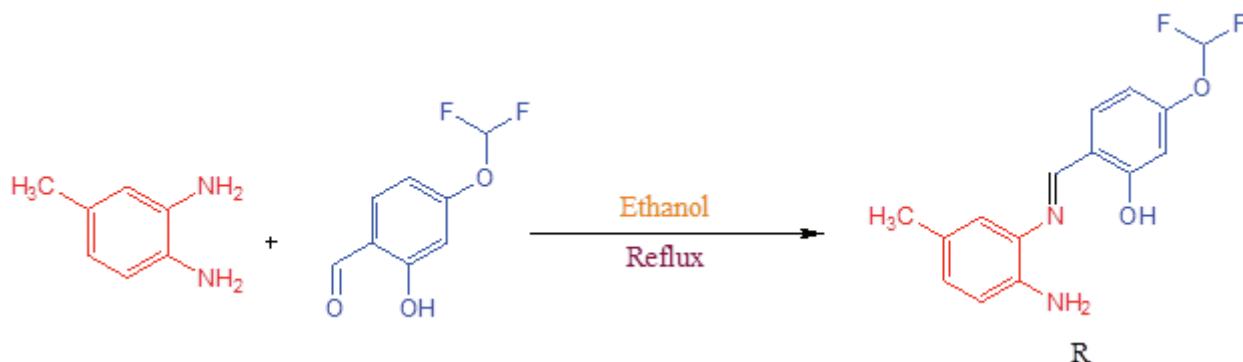
EXPERIMENTAL CHARACTERIZATION

Material and measurements

Most of the chemicals were bought from Sigma-Aldrich and were kept in the laboratory without further purification. Selective study of specific metal ions, including Ni^{2+} , Fe^{3+} , Cu^{2+} , Ca^{2+} , Co^{2+} , Mg^{2+} , Sn^{2+} , Ti^{2+} , Pb^{2+} , Zn^{2+} , Cd^{2+} , Hg^{2+} , Mn^{2+} , Al^{3+} , and Ag^+ , as well 1H & ^{13}C -NMR quantification were carried out on a Bruker spectrometer (1H & ^{13}C -NMR for 400 and 100 MHz), and the solvent used was dimethyl sulfoxide (DMSO). The UV–vis spectra were achieved using a UV-2450-Shimadzu spectrometer at room temperature by using the liquid compound mixing solution in distilled water and ethanol. The fluorescence emission spectra were determined on a spectrometer from Perkin Elmer LS45.

Synthesis of 2-((E)-(2-amino-5-methylphenylimino)methyl)-5-(difluoromethoxy)phenol (**R**)

A general protocol for the synthesized compound was followed, which is present in the literature. In a round-bottom flask, 4-methylbenzene-1,2-diamine (1 mmol) and 4-(difluoromethoxy)-2-hydroxybenzaldehyde (1 mmol) were dissolved in C_2H_5OH (20 ml). The mixed solutions were refluxed for 4 hours and maintained at $35^\circ C$ – $45^\circ C$. Afterward, the reaction was completed by cooling for a few hours at room temperature, and then the solution was poured into H_2O , forming a solid yellow solution. The solution was treated with H_2O , cleaned and then dried. The product was recrystallized from C_2H_5OH . Yield: 0.40 g, 70%. Melting point = $210^\circ C$; Fourier transform infrared spectroscopy (KBr), ν cm^{-1} 1,617, 1,606, 1,596 cm^{-1} (C=N), 3,056 cm^{-1} (Aromatic C-H), 3,415 cm^{-1} (OH), 3,184 cm^{-1} (NH_2), 1,108 cm^{-1} (O-HC-difluoro). 1H NMR (400 MHz DMSO- d_6): 12.710 (s, OH), 10.273 (s, NH), 7.792 (s, 1H), 7.788 (s, 1H), 7.591–7.565 (t, 3H J=10.4), 7.472–7.455 (d, 2H J=6.8), 7.360–7.340 (d, 2H J=8.0), 7.282–7.262 (d, 2H J=8.00), 7.153 (s, 1H), 7.032–7.011 (d, 2H J=8.4), 6.967 (s, 1H). ^{13}C (100 MHz, DMSO- d_6): 150.71, 149.48, 149.70, 140.25, 135.78, 128.99, 124.02, 122.42, 122.03, 119.63, 119.41, 118.37, 117.88, 117.06, 115.65, 115.65, 114.80, 114.49, 111.12, 56.50, 21.79,



Scheme 1. Synthesis of compound **R**.

19.02. electrospray ionization (ESI)-MS m/z : $[R-H^+ + Mg^{2+}]^+$ Calcd $[C_{16}H_{16}F_2N_2O]^+$, 290.12, found 292.00.

General procedure for spectral detection

The **R** stock solutions (10 μ M) were prepared by dissolving the amount needed in ethanol. All the metal cations, such as Mg^{2+} , Co^{2+} , Ni^{2+} , Cu^{2+} , Ca^{2+} , Sn^{2+} , Fe^{3+} , Ti^{2+} , Mn^{2+} , Pb^{2+} , Zn^{2+} , Cd^{2+} , Hg^{2+} , Al^{3+} , and Ag^+ (50 μ M), were dissolved in deionized H_2O for fluorescence and UV-vis absorption spectral analysis. Experiments with fluorescence and UV-vis titration were carried out using **R** (10 μ M) in 4-(2-hydroxyethyl)-1-piperazineethanesulfonic acid (HEPES) buffer (CH_3CH_2OH/H_2O , 1:4; v/v , pH 7.0). The metal sensing studies were carried out by tracking fluorescence and absorption spectral analyses. About 5-ml **R** solution (10 μ M) was packed into a 1-cm optical path length quartz cell and the concentration of Mg^{2+} (50 μ M) ions was gradually increased using a micropipette each time, with a 1-minute interval for complexation after each addition of Mg^{2+} ion.

Cell culture and cytotoxicity assays

HeLa cells were grown with 10% fasting blood sugar in Dulbecco's Modified Eagle's Medium. All the cells were treated with an antibiotic solution (0.1 mg ml^{-1} streptomycin, 0.25 mg ml^{-1} amphotericin B, and 100 units/ml penicillin) and grown under normal conditions at 37°C in cell culture (95% humidity, 5% CO_2 , respectively). In the culture media, the cells were seeded into 96-well plates at a density of 4×10^3 cells per well, and then compounds of 0, 7.8, 15.6, 31.2, 62.5, 125, 250, 500, 1,000, and 2,000 μ M (final concentration) were added. The cells were then incubated in an atmosphere of 5% CO_2 and 95% air for 24 hours, at 37°C. Enzyme-linked immunosorbent assay was used to measure the absorbance of the cells.

Molecular docking

The protein was first prepared using the protein preparation wizard and the docking experiments within Maestro 9.5 were conducted using Schrodinger's Glide program. Ligand preparation was carried out using LigPrep, followed by the minimization and optimization of the force field for liquid simulations (Dodda *et al.*, 2017). The G score was measured in kcal/mol, which included hydrogen bonds, internal strength, hydrophobic interactions, stacking interactions, ligand-protein interaction energies, and square deviation and desolvation of the center. The extra-precision (XP)'s glide module visualizes the specific interactions between ligands and proteins. Grids were developed using version 9.5 of Schrodinger's Glide following a standard procedure.

Theoretical calculation

The geometric optimization of receptor **R** and complex formation of Mg^{2+} provided lowest unoccupied molecular orbital (LUMO) and highest occupied molecular orbital (HOMO) energy gap values calculated by the density functional theory (DFT) using the B3LYP/6-31G level of the Gaussian 09 program. The receptor **R** and Mg^{2+} bind the complexes of chemosensor activity of alpha and beta value calculations, while the complexes are formed using the B3LYP/6-31G basis set of Mg^{2+} ions.

RESULTS AND DISCUSSION

The compound synthesized was 2-((E)-(2-amino-5-methylphenylimino)methyl)-5-(difluoromethoxy)phenol (**R**), which was characterized by FTIR, 1H & ^{13}C -NMR, and ESI-mass spectrometry. In order to calculate visual color change, the tests were determined under UV light. Moreover, the studies were persistent with the spectrofluorometric method to analyze the selectivity of specific metal ions, such as Ni^{2+} , Fe^{3+} , Ca^{2+} , Mn^{2+} , Cu^{2+} , Sn^{2+} , Mg^{2+} , Ti^{2+} , Co^{2+} , Pb^{2+} , Zn^{2+} , Cd^{2+} , Hg^{2+} , Al^{3+} , and Ag^+ .

UV-vis absorption spectroscopy

The studies on the absorption behavior of **R** (10 μ M) exhibited different metal ions, such as Cu^{2+} , Fe^{3+} , Co^{2+} , Ni^{2+} , Ca^{2+} , Sn^{2+} , Mg^{2+} , Ti^{2+} , Mn^{2+} , Pb^{2+} , Zn^{2+} , Cd^{2+} , Hg^{2+} , Al^{3+} , and Ag^+ (50 μ M) carried out in CH_3CH_2OH/H_2O , 1:4; v/v , (pH 7.0) with an absorption band at 320–378 nm as shown in Figure 1.

The UV-vis spectra of probe **R** showed major absorption peaks at 378 nm that can be attributed to π - π^* transition. Although various metal ions of 0.5 equiv. concentration were used, the interference of Mg^{2+} ions with probe **R** and the absorption intensity at 378 nm increased immediately and moved to a new absorption band at 415 nm. As shown in Fig. 2, solution **R** is colorless to light yellow, when seen by the naked eye. This is due to the presence of Mg^{2+} , which moves the absorption band in an upward direction at 378 nm. As shown in the UV-vis absorption spectrum (Fig. 3), the addition of Mg^{2+} ions (0.5 equiv.) increased the absorption strength from 378 nm to another peak at 415 nm, with two isosbestic points at 337 and 396 nm.

Fluorescence sensing of Mg^{2+}

The selectivity of receptor (sensor) **R** (10 μ M) for various metal ions, such as Ni^{2+} , Mn^{2+} , Fe^{3+} , Co^{2+} , Ca^{2+} , Mg^{2+} , Sn^{2+} , Cu^{2+} , Ti^{2+} , Pb^{2+} , Zn^{2+} , Cd^{2+} , Hg^{2+} , Al^{3+} , and Ag^+ (50 μ M) was

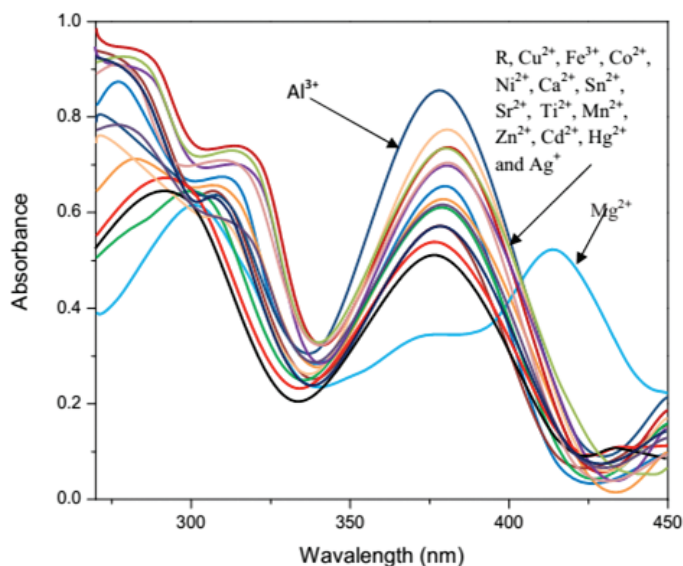


Figure 1. Absorption spectrum of **R** (10 μ M) upon addition of various metal ions (0.5 equiv. concentration used CH_3CH_2OH/H_2O , 1:4; v/v , pH 7.0).

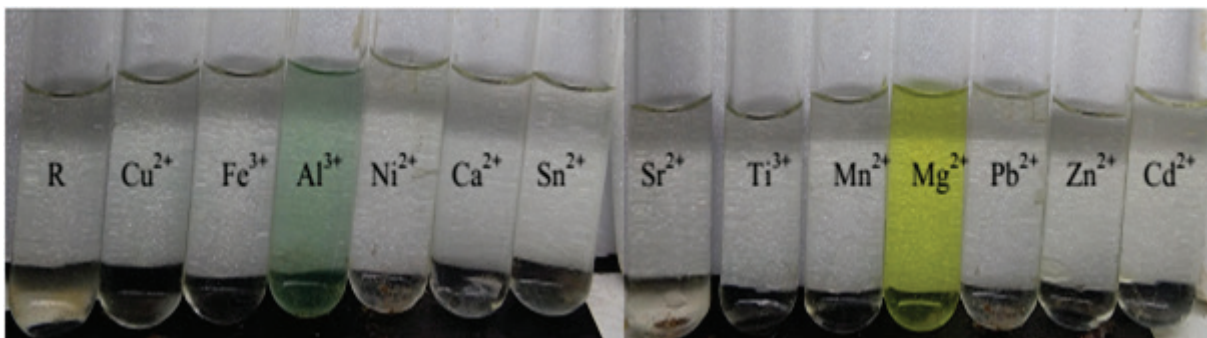


Figure 2. The different metal color solutions with sensing receptor **R** (10 μM) solution.

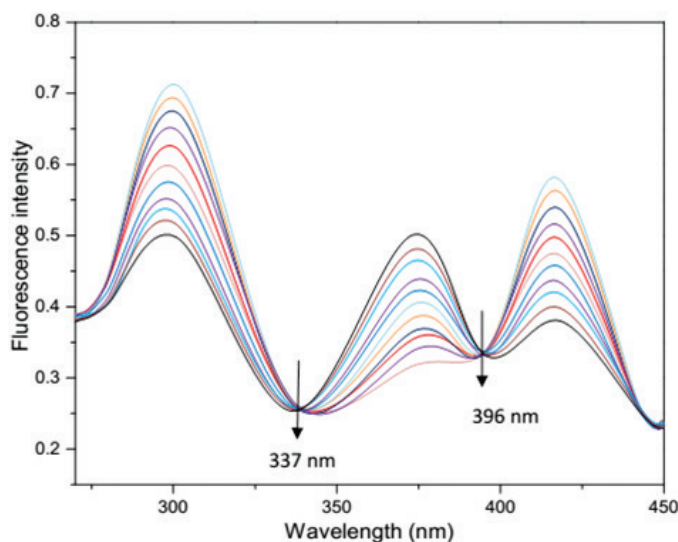


Figure 3. Absorbance spectrum of **R** (10 μM) upon addition of Mg^{2+} ions (0.5 equiv. response used; $\text{CH}_3\text{CH}_2\text{OH}/\text{H}_2\text{O}$, 1:4; v/v, pH 7.0).

investigated with $\text{CH}_3\text{CH}_2\text{OH}:\text{H}_2\text{O}$ solution (1:4, v/v, 20-mM HEPES buffer, pH 7.0) at room temperature. As shown in **Figure 4**, the fluorescence spectrum from 490 to 560 nm was obtained with an exciting value of 378 nm, and probe **R** (10 μM) exhibited an enhancement from weak emission intensity of fluorescence around at 524 nm due to selectivity and sensitivity of Mg^{2+} ions in the titration. Concomitantly, all the remaining metal ions showed no response for any emission changes. Probe **R** (10 μM) solution was induced by Mg^{2+} to change from blue to green, which determined the existence of Mg^{2+} as shown in **Figure 5**, under fluorescence light.

Furthermore, with the addition of Mg^{2+} ions of 5 equiv., the fluorescence emission intensity at 524 nm gradually increased as shown in **Figure 6**. The weak fluorescence intensity at 524 nm is assumed to be the intramolecular charge transfer of PET phenomenon caused by the intramolecular H bonding atom between $\text{C}=\text{N}$ and a hydroxyl group. As shown in **Scheme 2**, the fluorescence emission of the free **R** was feeble due to the lone pair electron of the N atom of the PET mechanism. The binding of **R**- Mg^{2+} complex resulted in the inhibition of PET and $-\text{CH}=\text{N}$

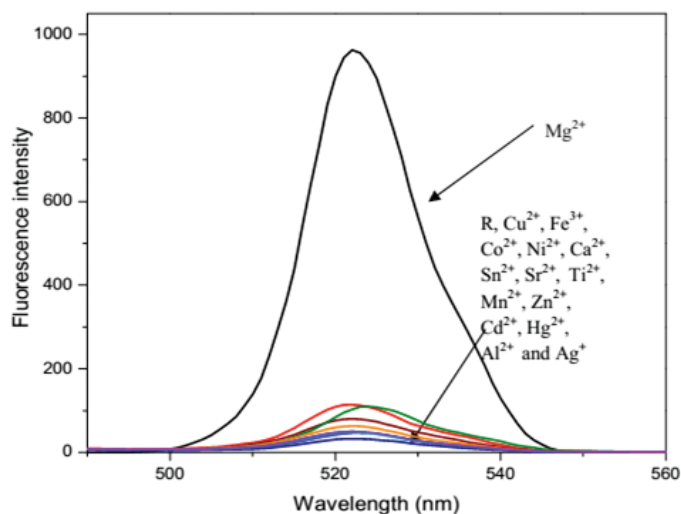


Figure 4. Fluorescence spectrum of **R** (20 μM) with different metal ions using the HEPES buffer solution ($\text{CH}_3\text{CH}_2\text{OH}/\text{H}_2\text{O}$, 1:4; v/v, pH 7.0).

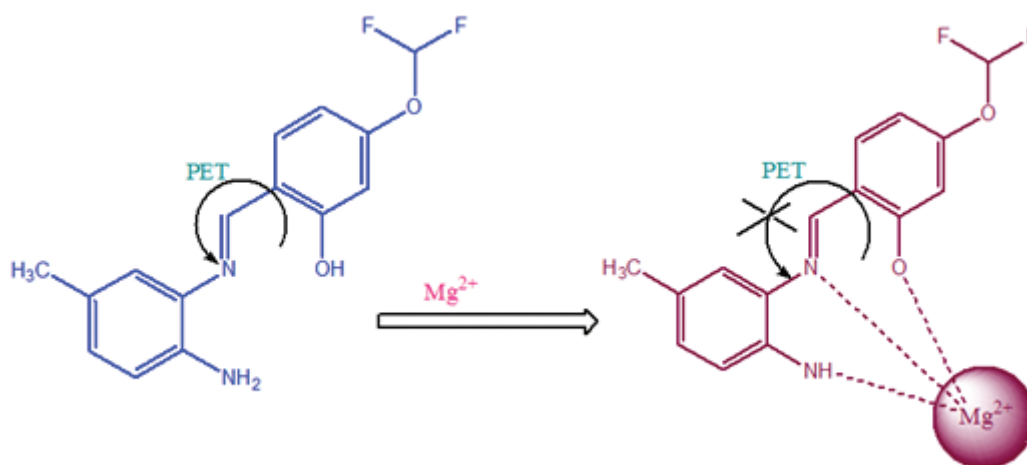
isomerization at the excited state, which remarkably increased the fluorescence emission intensity.

The stoichiometry between **R** and Mg^{2+} was determined using Job's plot with $\text{CH}_3\text{CH}_2\text{OH}/\text{H}_2\text{O}$ solution (1:4, v/v, 0.01 M HEPES buffer, pH 7.0) as shown in **Figure 7**. The fluorescence intensity at 524 nm calculated by a gradual increase in the maximum emission intensity of tested Mg^{2+} ions with 0.5 μM mole fraction indicated the 1:1 complex of the binding mode of **R** and Mg^{2+} . The result, further confirmed by the molecular peak ion at m/z 292.00, was assumed as $[\text{R}-\text{H}^++\text{Mg}^{2+}]^+$ (calculated m/z 289.00) in the ESI-Mass spectrum.

To further observe the attraction of **R** (10 μM) to Mg^{2+} (50 μM), competitive binding between Mg^{2+} and other metals to **R** (50 μM) was calibrated by using a mixed solution containing Mg^{2+} (50 μM) and each of the other metal cations, Hg^{2+} , Fe^{3+} , Co^{2+} , Zn^{2+} , Ni^{2+} , Cu^{2+} , Ca^{2+} , Sn^{2+} , Cd^{2+} , Mg^{2+} , Ti^{3+} , Mn^{2+} , Pb^{2+} , Al^{3+} , and Ag^+ (50 μM), in $\text{CH}_3\text{CH}_2\text{OH}:\text{H}_2\text{O}$ solution (1:4; v/v, 20-mM HEPES buffer, pH 7.0). From **Figure 8**, it is clear that all the competitive metal ions did not interact with the complex Mg^{2+} ion formation. Such findings show that no metal ions are influenced by the **R**- Mg^{2+} system.



Figure 5. Fluorescence sensing of different metal ions with **R** (10 μM) solution.



Scheme 2. Proposed mechanism of interaction of receptor **R** with Mg^{2+} ions.

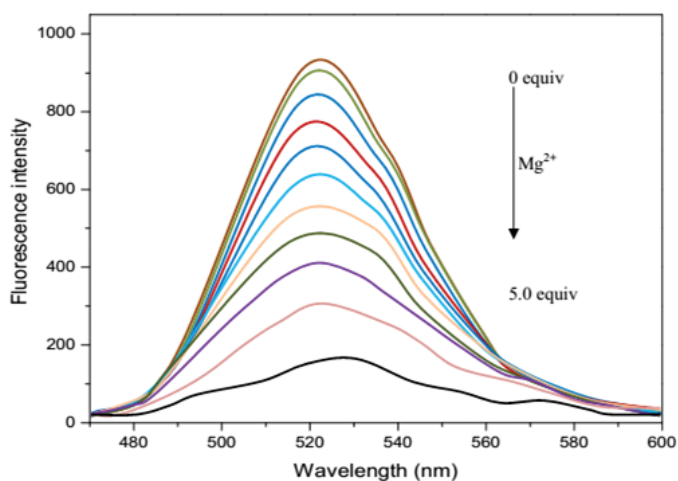


Figure 6. Fluorescence spectrum of **R** (10 μM) upon addition of Mg^{2+} ions (0.5 equiv. concentration of $\text{CH}_3\text{CH}_2\text{OH}/\text{H}_2\text{O}$, 1:4; v/v, pH 7.0).

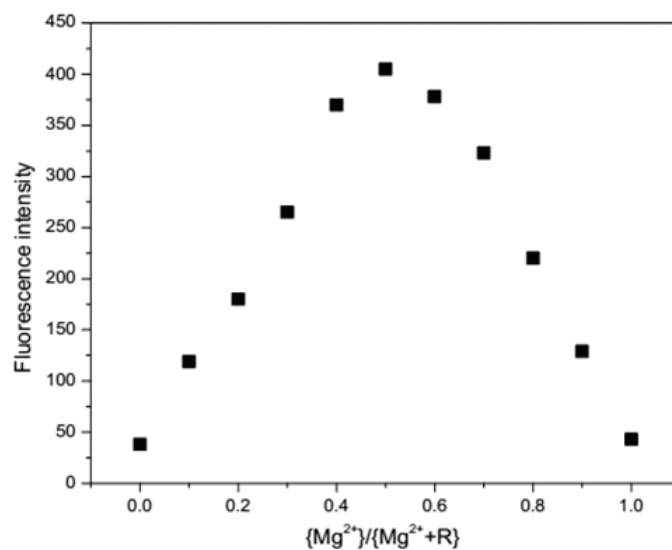


Figure 7. Job's plot of probe **R** (10 μM) with Mg^{2+} (50 μM) solution.

Effect of pH and binding reversibility

The pH titration implied as the optimal pH to sense metal ions and the spectrum is shown in Figure 9. The fluorescence emission of **R** was examined in the overall pH range, and from the figure it is evident that there is no change in the intensity and the existence of Mg^{2+} ion enhancement intensity of fluorescence at 524 nm in maximum at pH 7.0. In this experiment, pH 7.0 was

used for all measurements. EDTA (10 μM) solution was used to test the reversibility of sensor **R** (10 μM) binding with Mg^{2+} (50 μM) to validate novel chemosensors for practical use. Due to the binding receptor **R** and Mg^{2+} complexation, as shown in Figure 10, the turn-on fluorescence intensity was observed at 524 nm. The test revealed a strong **R**- Mg^{2+} complex fluorescence strength due

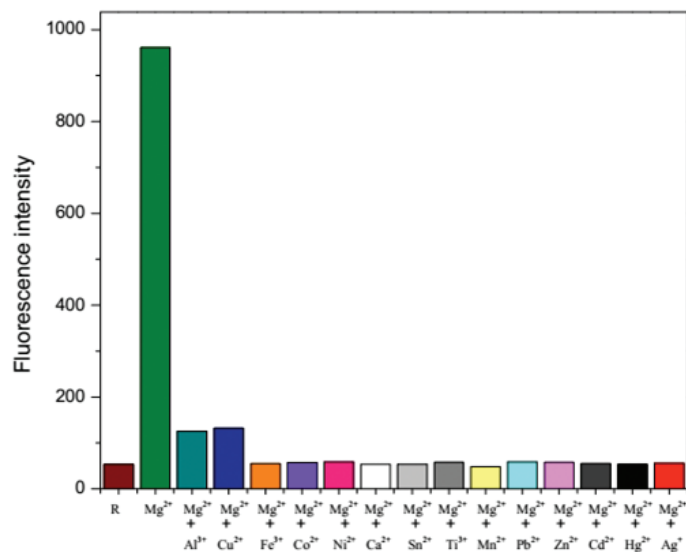


Figure 8. Competitive binding experiment of **R** toward Mg^{2+} in the presence of 5 equiv. of other metal cations.

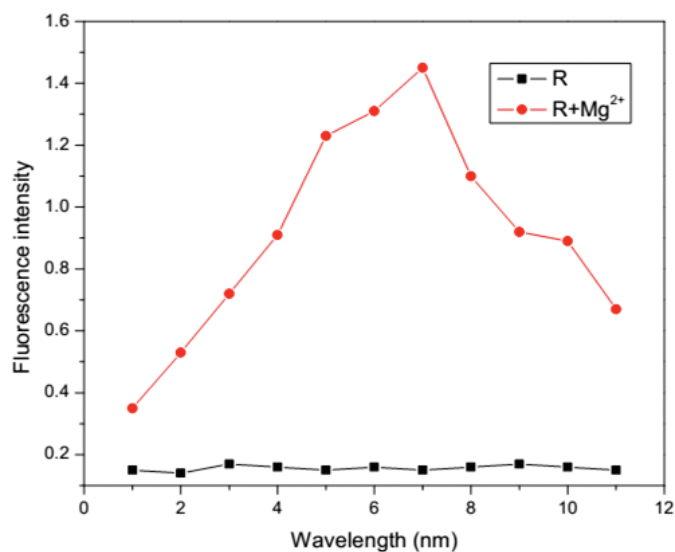


Figure 10. The fluorescence intensity of **R** ($10 \mu M$) with **R**- Mg^{2+} complex used different pH values. Excitation and emission wavelengths were at 324 and 524 nm, respectively.

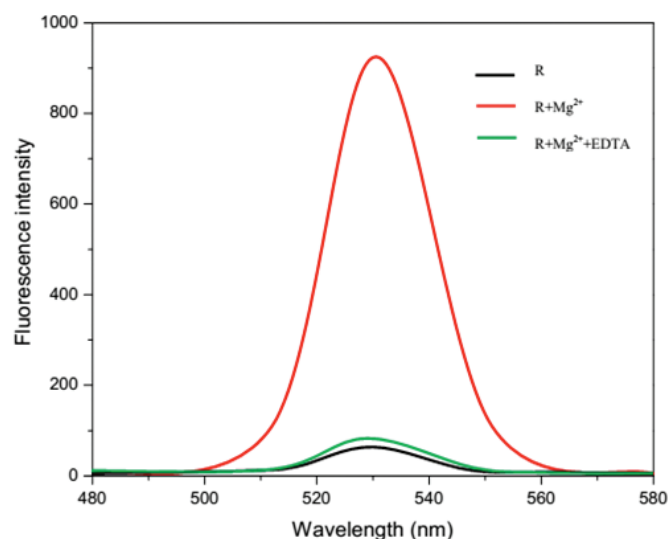


Figure 9. The fluorescence spectrum of **R** ($10 \mu M$) binding with **R**- Mg^{2+} and **R**- Mg^{2+} +EDTA solution (CH_3CH_2OH/H_2O , 1:4; v/v, pH 7.0).

to the presence of Mg^{2+} ion. Although **R**- Mg^{2+} -EDTA complex did not promote high intensity, it showed the reversibility of receptor **R** to Mg^{2+} ions.

The cytotoxicity activity

With the HeLa cell line, the cytotoxicity effects of **R** can be estimated. The IC_{50} values of this assay for the HeLa cells were obtained by conducting the cell viability experiment by treatment with compound-varying concentrations. **Figure 11** shows the cytotoxicity analyses of the HeLa cell line with specific ligand preparation concentrations. HeLa cells were treated with ligand **R** for about 36 hours (**Figure 11b** and **c**), and the empty cells can be seen in **Figure 11a**. The ligand **R** was used to treat HeLa cells with respect to different concentrations to analyze the cytotoxic activity.

The cell viability (%) of the ligand and its various concentrations (**Dhineshkumar et al.**, 2019) with its respective IC_{50} values are given in **Table 1**. Plots of the HeLa cell line viability and the concentration of the ligand treatment are shown in **Figure 12**.

The IC_{50} values of the inhibited cells take up much time. From this experiment, the key recovery mechanism for unaccepted aspects effects the rationalization of the IC_{50} values with short time intervals.

Molecular docking

In an attempt to understand our compound's binding mode, the ligand was docked by the Protein Data Bank with the crystal structure of the FGF receptor two kinases [protein data bank (PDB):4J96]. The protein was first prepared using the protein preparation wizard, and the docking experiments were conducted using the XP mode of the Schrodinger Glide program (Maestro 9.5). The 2D diagram interactions of active compounds are shown in **Figure 13**. From the docking studies, we find that the compound showed the highest G scores comparatively with others. **Figure 14** shows a composite 3D model in the complex.

Theoretical studies

In order to gain an insight into the binding mode of receptor **R** fluorescence-sensing mechanism against Mg^{2+} , DFT calculations at the B3LYP/6-31G level using Gaussian 09 software were carried out to recognize the optimized structures of **R** and its Mg^{2+} complex. The optimized molecular structure of probe **R** and **R**- Mg^{2+} exhibited in the ground state was computed by the B3LYP calculation with a 6-31G (d,p) basis set as shown in **Figure 15**. The electron density distributions and orbital energy transfer from the HOMO and LUMO investigated the probe **R** and **R**- Mg^{2+} complex.

Although sensor **R** and the HOMO electron densities were primarily located on the hydroxyl group and replaced the

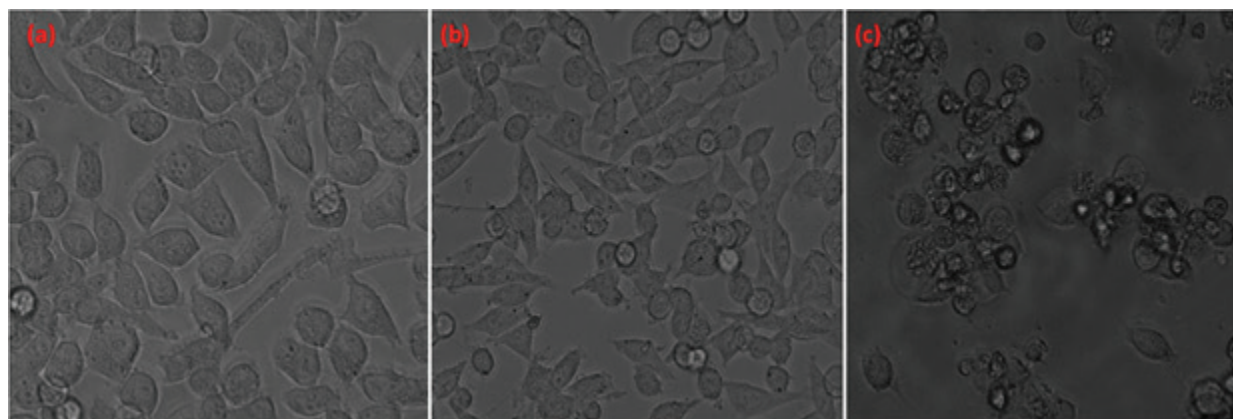


Figure 11. The cytotoxicity activity of HeLa cells with ligand. (a) Empty cells, (b) after treatment of some cells, and (c) whole cells treated after testing with the compound.

Table 1. Anticancer activity cell viability.

HeLa cells		IC ₅₀ values
Concentration (μM)		R
0		100
7.8		89.47
15.6		78.8
31.2		69.22
62.5		52.34
125		47.2
250		33.49
500		21.83
1,000		11.09
2,000		5.4

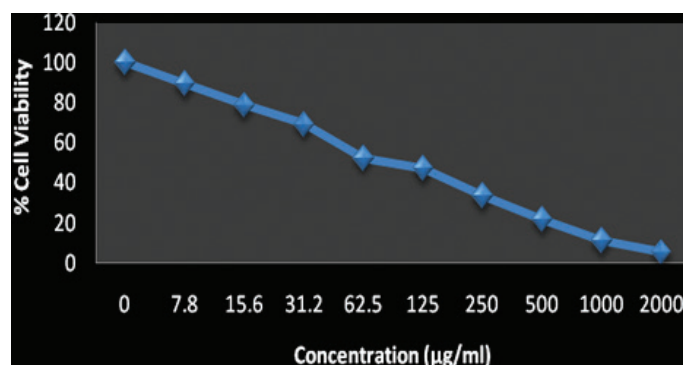


Figure 12. The cell viability with various concentrations of HeLa cells (0–2,000 μM).

amine group, the transfer of 4-(2,2-difluoroethyl)-2-hydroxy benzaldehyde group occurred through LUMO orbital energies. It was an electron transfer that contributed to the energy level from HOMO to LUMO. However, the imine group of C=N isomerization and PET of probe **R** may also be responsible for fluorescent nature in the coordinate complex 1:1 ratio (Dhineshkumar *et al.*, 2018).

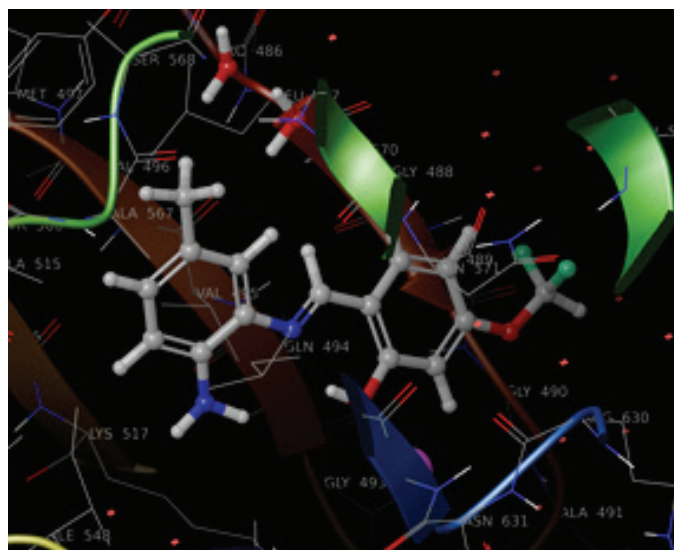


Figure 13. 3D mode of the compound receptor **R** with the binding site.

Optimized theoretical calculations were conducted to calculate the coordinated sensor **R** to **R**-Mg²⁺ complex and the energy levels of both the LUMO and HOMO energy gap values (Figure 16).

The sensor **R** showed that HOMO (5.40 eV) and LUMO (3.12 eV) orbital energies were completely involved in working together in ligand-to-ligand charge transfer with a bandgap of 3.48 eV. The mechanism of 1:1 stoichiometry of equal binding with **R**-Mg²⁺ predicts that HOMO and LUMO can be assumed as alpha and beta, HOMO_{Alpha} = 3.12 eV and LUMO_{Alpha} = 1.69 eV with calculated energy gap at 1.43 eV, while HOMO_{Beta} = 5.40 eV and LUMO_{Beta} = 1.68 eV with calculated energy gap at 3.72 eV. The metal complex formed with **R**-Mg²⁺ exhibited an alpha value with a low energy gap and the beta value exhibited a high energy gap. The **R**-Mg²⁺ complex bound by the imine group (-C=N) and hydroxyl group had a strong bond formation due to elimination of the PET process on turn-on fluorescence. As a result, sensor **R** exhibited an electronegativity attractive value of 3.101 eV. While electrophilicity

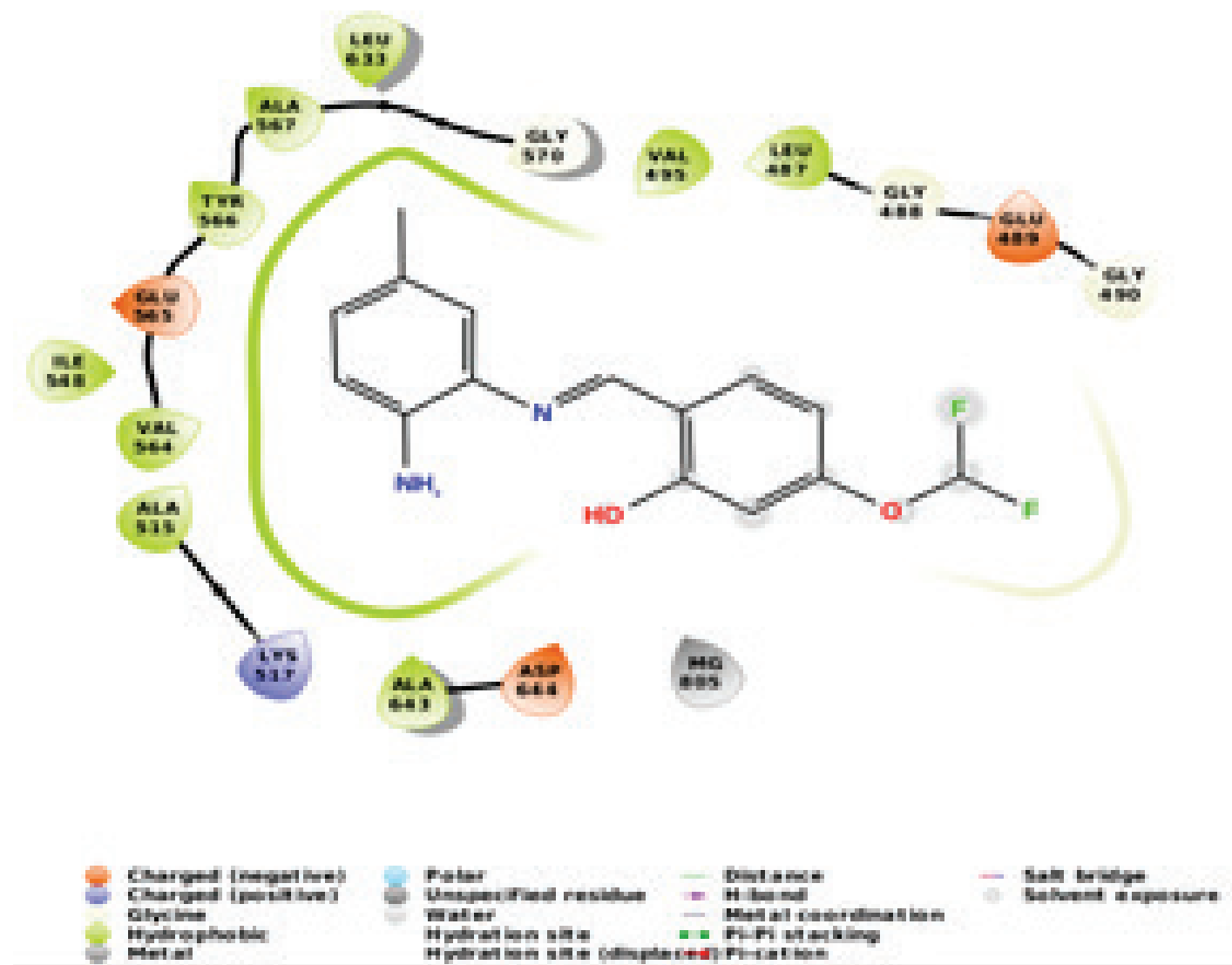


Figure 14. 2D binding activity of compound receptor R.

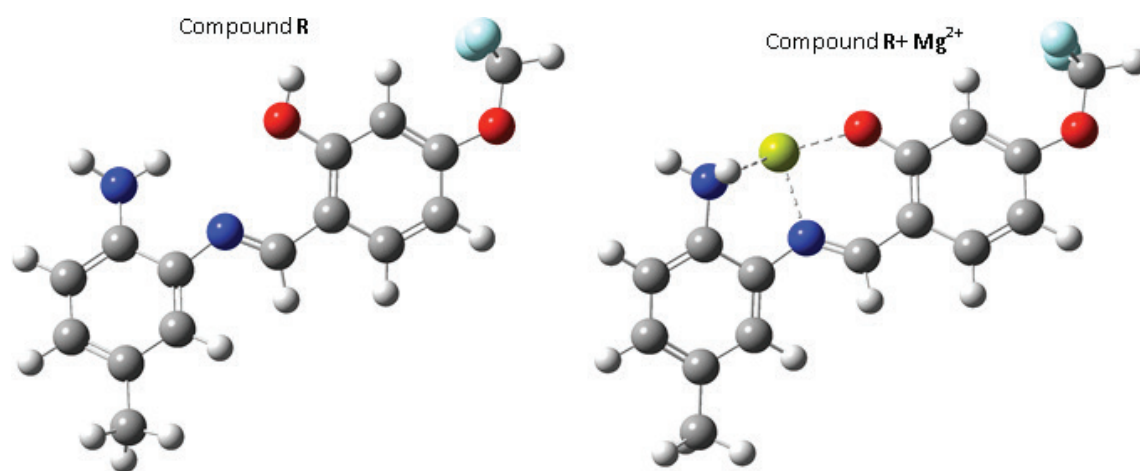


Figure 15. Optimized molecular structure of ligand R and R-Mg²⁺.

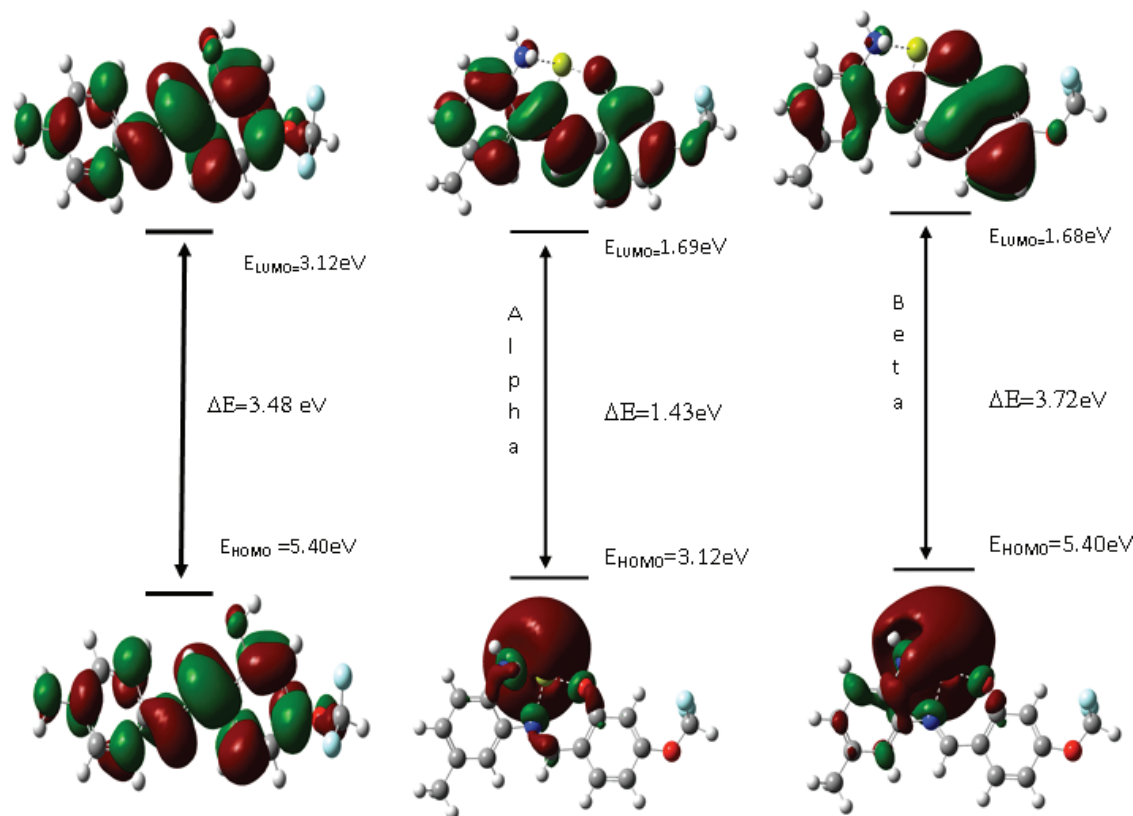


Figure 16. Optimized structural geometry of chemosensors and its complexes **R** and **R-Mg²⁺** from left to right.

Table 2. Dipole moment (Debye), Polarisibility (a.u), and Hyperpolarisibility (a.u).

Dipole moment (Debye)		Polarisibility (a.u)		Hyperpolarisibility (a.u)	
Parameter	Value	Parameter	Value	Parameter	Value
μ_x	-0.8588	α_{xx}	104.51	β_{xxx}	105.3128
μ_y	1.4393	α_{yy}	103.76	β_{yyy}	23.9069
μ_z	-1.0599	α_{zz}	125.01	β_{zzz}	15.2604
μ_{total}	1.9831	α_{xy}	1.42	β_{xyy}	29.9064
		α_{xz}	1.72	β_{xxy}	-17.258
		α_{yz}	0.64	β_{xxz}	-55.115
		α_o (esu) $\times 10^{-23}$	1.65	β_{zzz}	36.181
		$\Delta\alpha$ (esu) $\times 10^{-24}$	3.99	β_{yzz}	2.5332
				β_{yyz}	5.0227
				β_{xyz}	22.312
				β_o (esu) $\times 10^{-30}$	1.96

electron pair acceptor value stood at 2.763 eV, hardness and softness values were obtained between 1.7405 and 0.2872 eV. The receptor **R**, LUMO, and HOMO energy values of hyperpolarizability, polarizability, and dipole moment are presented in Table 2.

Charge distribution

Gaussian program of Mulliken method using a B3LYP/6-31G level calculation was used to calculate the charge distribution of the molecule. In this molecule, every atom charge distribution calculation was delineated. The bond length between atoms are shown by increasing and decreasing the distribution of negative

and positive charges, and Mulliken atomic charge values and plots are shown in Figure 17. The Mulliken value with the negative charge for the high and low carbon groups, such as C16, C15, C13, C11, C12, C10, C9, C7, C6, C5, C4, C3, C2, and C1 atoms, and the N8, O14, F15, and O16 atoms in compound **R**, are also shown. The hydrogen atoms were split with fluorine atoms and linked to oxygen atoms, while all the remaining hydrogen atom were split with their positions. Mulliken charge was based on estimating calculation partial atomic charges from the computational chemistry in working Mulliken population analysis (Arockia doss *et al.*, 2020; Dhineshkumar *et al.*, 2020).

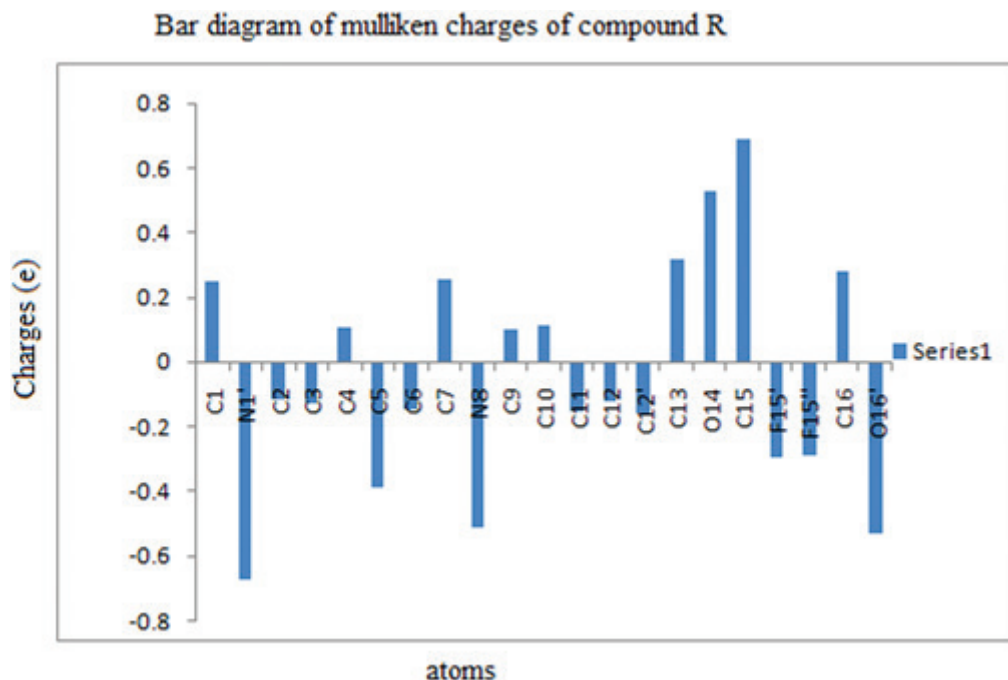


Figure 17. Mulliken atomic charges for R.

CONCLUSION

In summary, the Schiff base of 2-((E)-(2-amino-5-methylphenylimino)methyl)-5 (difluoromethoxy)phenol was synthesized and investigated by analytical techniques. The sensitivity and selectivity of Mg^{2+} ions due to fluorescence emission intensity at 524 nm was ascertained by other metal ions, with an excitation wavelength at 378 nm. The stoichiometry of 1:1 complex was recognized for mole fraction of 0.5. The receptor R and the existence of Mg^{2+} ions in the R- Mg^{2+} complex was confirmed by the turn-on fluorescence mass spectra and EDTA titration. Furthermore, different pH's used confirm the optimum pH. The cytotoxicity effect of inhibition strong force to HeLa cells was analyzed with the compound. Molecular docking of PDB: 4J96 protein was also studied for this compound.

AUTHOR CONTRIBUTIONS

CAS and EDK conceptualized, designed, and finalized Schemes 1 and 2. CAS, EDK, and MY carried out the research work and wrote the article. All the authors read and agreed to published this version of the manuscript.

CONFLICT OF INTEREST

All the authors declare that there are no conflicts of interest.

FUNDING

This research received no external funding.

REFERENCES

Abu-Dief AM, Mohamed IMA. A review on versatile applications of transition metal complexes incorporating Schiff bases. Beni Suf Univ J Basic Appl Sci, 2015; 4:119–33.

Adsule S, Barve V, Chen D, Ahmed F, Dou QP, Padhye S, Sarkar FH. Novel Schiff base copper complexes of quinoline-2 carboxaldehyde as proteasome inhibitors in human prostate cancer cells. J Med Chem, 2006; 49:7242–6.

Arockia doss M, Rajarajan G, Dhineshkumar E, Amala S, Thanikachalam V, Selvanayagam S, Sridhar B. Synthesis, spectral characterization (FT-IR, NMR, XRD) and computational studies of chloroacetyl chloride incorporated 3t-butyl-2r,6c-diphenyl/di(thiophen-2-yl)piperidin-4-ones. J Mol Struct, 2020; 1200:127076.

Beer PD. Transition-metal receptor systems for the selective recognition and sensing of anionic guest species. Acc Chem Res, 1998; 31:71–80.

Cozzi PG, Dolci LS, Garelli A, Montalti M, Prodi L, Zaccheroni N. Photophysical properties of Schiff-base metal complexes. New J Chem, 2003; 27:692–7.

Dhineshkumar E, Iyappan M, Anbuselvan C. A novel dual chemosensor for selective heavy metal ions Al^{3+} , Cr^{3+} and its applicable cytotoxic activity, HepG2 living cell images and theoretical studies. J Mol Struct, 2020; 1210:128033.

Dhineshkumar E, Iyappan M, Anbuselvan C. Limiting clutches for 'turn-on' and 'turn-off' chemosensors of 1,2-bis((E)-9-anthracenyl)methyleneamino)-9,10-anthraquinone. J Mol Struct, 2019; 1177:545–57.

Dhineshkumar E, Iyappan M, Anbuselvan C. Turn on macrocyclic chemosensor for Al^{3+} ion with facile synthesis and application in live cell imaging. Spectrochim Acta Part A Mol Biomol Spectrosc, 2018; 199:209–19.

Dodda LS, Cabeza de Vaca I, Tirado-Rives J, Jorgensen WL. LigParGen web server: an automatic OPLS-AA parameter generator for organic ligands. Nucl Acids Res, 2017; 45(W1):W331–6.

Gao Z, Feng H, Wang S, Huang Y, Ren X, Pang L, Hu S. Fluorescence turn-on of salicylaldehyde ligands by co-ordination with magnesium and amines. New J Chem, 2018; 42:18513–6.

Gupta AS, Paul K, Luxami V. A new 'Turn-on' PET-CHEF based fluorescent sensor for Al^{3+} and CN^{-} ions: applications in real samples. Anal Methods, 2018; 10:983–90.

Jana A, Das B, Mandal SK, Mabhai S, Khuda-Bukhsh AR, Dey S. Deciphering the CHEF-PET-ESIPT liaison mechanism in a Zn²⁺ chemosensor and its applications in cell imaging study. *New J Chem*, 2016; 40:5976–84.

Jia Y, Li J. Molecular assembly of Schiff base interactions: construction and application. *Chem Rev*, 2015; 115:1597–621.

Kim MJ, Konduri R, Ye H, MacDonnell FM, Puntoriero F, Serroni S, Campagna S, Holder T, Kinsel G, Rajeshwar K. Dinuclear ruthenium(II) polypyridyl complexes containing large, redox-active, aromatic bridging ligands: synthesis, characterization, and intramolecular quenching of MLCT excited states. *Inorg Chem*, 2002; 41:2471–6.

Kim SK, Yoon J. A new fluorescent PET chemosensor for fluoride ions dedicated to the memory of D. J. Cram. *Chem Commun*, 2002; 7:770–1.

Li Y, Wu J, Jin X, Wang J, Han S, Wu W, Xu J, Liu W, Yao X, Tang Y. A bimodal multianalyte simple molecule chemosensor for Mg²⁺, Zn²⁺, and Co²⁺. *Dalton Trans*, 2014; 43:1881–7.

Li Y, Yang Z. DNA binding affinity and antioxidative activity of copper(II) and zinc(II) complexes with a novel hesperetin Schiff base ligand. *Inorganica Chim Acta*, 2009; 362:4823–31.

Liu M, Yu X, Li M, Liao N, Bi A, Jiang Y, Liu S, Gong Z, Zeng W. Fluorescent probes for the detection of magnesium ions (Mg²⁺): from design to application. *RSC Adv*, 2018; 8:12573–87.

Liu YC, Yang ZY. Antioxidation and DNA binding properties of binuclear Nd(III) complexes with Schiff-base ligands derived from 8-hydroxyquinoline-2-carboxyaldehyde and four aroylhydrazides. *Inorg Chem Commun*, 2009; 12:704–6.

Men G, Chen C, Zhang S, Liang C, Wang Y, Deng M, Shang H, Yang B, Jiang S. A real-time fluorescent sensor specific to Mg²⁺: crystallographic evidence, DFT calculation and its use for quantitative determination of magnesium in drinking water. *Dalton Trans*, 2015; 44: 2755–62.

Mouri S, Chen Z, Mitsunuma H, Furutachi M, Matsunaga S, Shibasaki M. Catalytic asymmetric synthesis of 3-Aminooxindoles: enantiofacial selectivity switch in bimetallic vs monometallic Schiff base catalysis. *J Am Chem Soc*, 2010; 132:1255–7.

Orrego-Hernández J, Nuñez-Dallos N, Portilla J. Recognition of Mg²⁺ by a new fluorescent ‘turn-on’ chemosensor based on pyridyl-hydrazono-coumarin. *Talanta*, 2016; 152:432–7.

Parashar RK, Sharma RC, Kumar A, Mohan G. Stability studies in relation to IR data of some schiff base complexes of transition metals and their biological and pharmacological studies. *Inorganica Chim Acta*, 1988; 151:201–8.

Raman N, Kulandaisamy A, Shunmugasundaram A, Jeyasubramanian K. Synthesis, spectral, redox and antimicrobial activities of Schiff base complexes derived from 1-phenyl-2,3-dimethyl-4-aminopyrazol-5-one and acetoacetanilide. *Transit Metal Chem*, 2001; 26:131–5.

Tamil Selvan G, Chitra V, Enoch Israel VMV, Selvakumar PM. Development of a fluorescent chemosensor towards sensing and separation of Mg²⁺ ions in chlorophyll and hard water. *New J Chem*, 2018; 42:902–9.

Tarafder MT, Kasbollah A, Crouse K, Ali A, Yamin B, Fun HK. Synthesis and characterization of Zn(II) and Cd(II) complexes of S-benzyl-β-N-(2-pyridyl) methylenedithiocarbamate (HNNS): bioactivity of the HNNS Schiff base and its Zn(II), Cu(II) and Cd(II) complexes and the X-ray structure of the [Zn(NNS)₂] complex. *Polyhedron*, 2001; 20:2363–70.

Treadwell R, de Moliner F, Subiros-Funosas R, Hurd T, Knox K, Vendrell M. A fluorescent activatable probe for imaging intracellular Mg²⁺. *Org Biomol Chem*, 2018; 16:239–44.

Wu JS, Liu WM, Zhuang XQ, Wang F, Wang PF, Tao SL, Zhang XH, Wu SK, Lee ST. Fluorescence turn on of coumarin derivatives by metal cations: a new signaling mechanism based on C=N isomerization. *Org Lett*, 2007; 9:33–6.

Xu Z, Qian X, Cui J. Colorimetric and ratiometric fluorescent chemosensor with a large red-shift in emission: Cu(II)-Only sensing by deprotonation of secondary amines as receptor conjugated to naphthalimide fluorophore. *Org Lett*, 2005; 7:3029–32.

Zhao L, Liu Y, He C, Wang J, Duan C. Coordination-driven nanosized lanthanide ‘Molecular Lanterns’ as luminescent chemosensors for the selective sensing of magnesium ions. *Dalton Trans*, 2014; 43:335–43.

Ziółek M, Filipczak K, Maciejewski A. Spectroscopic and photophysical properties of salicylaldehyde azine (SAA) as a photochromic Schiff base suitable for heterogeneous studies. *Chem Phys Lett*, 2008; 464:181–6.

How to cite this article:

Mathivanan I, Ezhumalai D, Chinnadurai A. A Schiff base of 2-((E)-(2-amino-5-methylphenylimino)methyl)-5-(difluoromethoxy)phenol and its applications of fluorescent chemosensor for selective of Mg²⁺ ion, molecular docking and anticancer activity. *J Appl Pharm Sci*, 2020; 10(08):075–085.